Quantitative Mapping of Collagen Fiber Orientation in Non-glaucoma and Glaucoma Posterior Human Sclerae

Jacek K. Pijanka,[1] *Baptiste Coudrillier,*[2] *Kimberly Ziegler,*[2] *Thomas Sorensen,*[3] *Keith M. Meek,*[1] *Thao D. Nguyen,*[2] *Harry A. Quigley,*[4] *and Craig Boote*[1]

Purpose. The posterior sclera has a major biomechanical influence on the optic nerve head, and may therefore be important in glaucoma. Scleral material properties are influenced significantly by collagen fiber architecture. Here we quantitatively map fiber orientation in non-glaucoma and glaucoma posterior human sclerae.

Methods. Wide-angle x-ray scattering quantified fiber orientation at 0.5-mm intervals across seven non-glaucoma postmortem human sclerae, and five sclerae with glaucoma history and confirmed axon loss. Multiphoton microscopy provided semiquantitative depth-profiling in the peripapillary sclera.

Results. Midposterior fiber orientation was either uniaxial (one preferred direction) or biaxial (two directions). The peripapillary sclera was characterized by a ring of fibers located mainly in the mid-/outer stromal depth and encompassing ~50% of the total tissue thickness. Fiber anisotropy was 37% higher in the peripapillary sclera compared with midposterior, varied up to 4-fold with position around the scleral canal, and was consistently lowest in the superior-nasal quadrant. Mean fiber anisotropy was significantly lower in the superior-temporal ($P < 0.01$) and inferior-nasal ($P < 0.05$) peripapillary scleral quadrants in glaucoma compared with non-glaucoma eyes.

Conclusions. The collagen fiber architecture of the posterior human sclera is highly anisotropic and inhomogeneous. Regional differences in peripapillary fiber anisotropy between non-glaucoma and glaucoma eyes may represent adaptive changes in response to elevated IOP and/or glaucoma, or baseline structural properties that associate with predisposition to glaucomatous axon damage. Quantitative fiber orientation data will benefit numerical eye models aimed at predicting the sclera's influence on nerve head biomechanics, and thereby its possible role in glaucoma. (*Invest Ophthalmol Vis Sci.* 2012;53:5258–5270) DOI:10.1167/iovs.12-9705

[1]From the Structural Biophysics Group, School of Optometry and Vision Sciences, Cardiff University, Cardiff, United Kingdom; the [2]Department of Mechanical Engineering, Johns Hopkins University, Baltimore, Maryland; [3]Diamond Light Source, Didcot, United Kingdom; and the [4]Glaucoma Center of Excellence, Wilmer Ophthalmological Institute, Johns Hopkins University School of Medicine, Baltimore, Maryland.

Presented at the annual meeting of the Association for Research in Vision and Ophthalmology, Fort Lauderdale, Florida, May 2010.

Supported by Fight for Sight Grant 1360; NIH Grants EY021500, EY02120, and EY01765; and USAMRMC Award W81XWH-10-1-0766.

Submitted for publication February 15, 2012; revised April 27 and May 31, 2012; accepted July 2, 2012.

Disclosure: **J.K. Pijanka**, None; **B. Coudrillier**, None; **K. Ziegler**, None; **T. Sorensen**, None; **K.M. Meek**, None; **T.D. Nguyen**, None; **H.A. Quigley**, None; **C. Boote**, None

Corresponding author: Craig Boote, Structural Biophysics Group, School of Optometry and Vision Sciences, Cardiff University, Maindy Road, Cardiff CF24 4LU, UK; bootec@cf.ac.uk.

The sclera forms approximately 85% of the eye's outer tunic in humans, providing a tough, fibrous supporting substrate for the other ocular components including the retina and optic nerve head. A complex network of collagen fibers forms the sclera's major load-carrying component,[1] and is a major influence on the tissue's biomechanical response to changes in IOP.[2] Accurate, quantitative information on scleral fiber architecture will therefore be important in order to understand and model the tissue's physiological load-bearing behavior and its clinical implications.

In the biomechanical paradigm of glaucoma, it is proposed that IOP-induced deformation in and around the lamina cribrosa initiates a complex cascade of events that ultimately result in ganglion cell dysfunction and apoptosis.[3,4] The physical effects of IOP on nerve axons as they traverse the lamina are transmitted both directly via the trans-lamina pressure differential, and also indirectly via the supporting tissues of the eye-wall, of which the sclera is paramount as the main stress-bearing tissue.[2,5–8] While the properties of the lamina itself—as the main injury site[9]—are important in glaucoma, recent research suggests that the mechanical influence of the surrounding sclera may also be key. Modeling studies have indicated that scleral shape, thickness, and material properties are all influential factors,[5–7,10] and that posterior scleral stiffness is a major material determinant of IOP-derived lamina strain.[7] In addition, alterations in tissue thickness,[11] mechanics,[12,13] and matrix ultrastructure[14,15] in human and experimental glaucoma suggest a role for the peripapillary sclera in the disease mechanism.

A number of techniques have provided information on the arrangement of scleral collagen. Using histological reconstructions, Kokott was the first to suggest, over 75 years ago, that the posterior scleral fibers adopt preferred orientations that may relate to physical forces acting on the globe.[16] A number of imaging tools have provided more recent insight, including transmission[17] and scanning[18] electron microscopy, atomic force microscopy,[18] and second harmonic generation multiphoton microscopy.[19,20] However, these studies, while important, have provided largely qualitative and/or localized information. Most recently, small-angle light scattering has been used to quantify fiber orientation in rat sclera.[21] This method has also yielded valuable information on human tissue, albeit these measurements were restricted to the temporal region of the peripapillary sclera.[19] Thus, extensive, quantitative information on collagen fiber orientation in the human sclera is still lacking in the literature.

We have developed a method, based on wide-angle-angle x-ray scattering (WAXS), which provides quantitative measurements of bulk collagen fiber orientation in situ, without the need for tissue processing that may perturb the native tissue structure. Previously we have applied this method to map fiber orientation in the cornea and the ~3 mm of sclera adjacent to the limbus (reviewed[22]). However, up until now WAXS has not been employed in studies of the posterior sclera. In the current

paper, our aim was to apply this technique to quantitatively map collagen fiber orientation in non-glaucoma and glaucoma posterior human sclerae.

Methods

Tissue Details

All experimental procedures were performed in accordance with the Declaration of Helsinki. Non-glaucoma and glaucoma human eyes, all from Caucasian donors, were obtained from the National Disease Research Interchange (NDRI) within 48 hours post-mortem. Eyes were shipped on dry ice and preserved in balanced salt solution (BSS; Alcon, Inc., Fort Worth, TX). A provisional designation of glaucoma was made on the basis of either having an extensive history in the office of one of the authors (HAQ) premortem (donor g1), or where post-mortem medical records showed a coded diagnosis of glaucoma by virtue of a documented prescription of known IOP-lowering medications and/or where the family confirmed that the donor had been treated for glaucoma. Provisional non-glaucoma status was assigned where a specimen met none of these criteria. None of the eyes used in this study had any previous history of ocular surgery involving the posterior sclera.

Specimen Preparation

The surrounding fat, muscle, and episcleral tissues were gently removed from each eye, and the optic nerve excised with a razor blade flush to the sclera and preserved in 4% paraformaldehyde (Electron Microscopy Sciences, Hatfield, PA) for subsequent axon loss grading. While keeping the intact eyes moist with BSS, the axial length and the nasal-temporal and superior-inferior globe diameters were measured using digital calipers. The cornea and anterior sclera were then excised and the lens, retina, and choroid removed. The intact posterior sclerae were stored in 4% paraformaldehyde at 4°C until the time of x-ray experiments. Our previous work has shown that this mild fixation method does not affect WAXS collagen orientation measurements.[23]

Optic Nerve Grading

To confirm the provisional glaucoma diagnosis, cross-sections were taken from each fixed optic nerve at locations 1–3 mm behind the eye, embedded in epoxy resin, and sectioned at 1-μm thickness. A glaucoma specialist (HAQ), experienced in optic nerve grading and masked to the provisional diagnosis, then assigned a quantitative grade from 0 to 3 for the degree of axon loss,[12,24] where: Grade 0 was <10% loss (normal); Grade 1 was 10% to 25% loss (mild); Grade 2 was 25% to 50% loss (intermediate); Grade 3 was 50% to 75% loss (severe). All non-glaucoma eyes were confirmed to have a grading of 0 (normal), while only glaucoma eyes receiving a grading of 2 or 3 (intermediate/severe) were used in subsequent experiments. The resulting number of eyes available for WAXS was seven non-glaucoma (from six donors) and five glaucoma (from four donors). The mean age of the non-glaucoma eyes was 76 (± 7) years, and the mean age of the glaucoma eyes was 75 (± 10) years. Details of all the eyes used are given in Table 1.

X-ray Scattering

X-ray scattering experiments were carried out on a diffraction beamline (Beamline I02; Diamond Light Source Ltd, Oxfordshire, UK) at the Diamond Light Source (Didcot), the UK's national synchrotron facility. Immediately prior to x-ray exposure, a 15-mm circular specimen, centered on the optic nerve head, was excised from each intact fixed posterior sclera; wrapped in polyvinylidene chloride film to prevent tissue dehydration throughout the duration of the data collection (~1.5 hrs per specimen); and mounted inside acrylic plastic (Perspex; Lucite Group Ltd, Southampton, UK) chambers with Mylar (DuPont-Teijin, Middleborough, UK) windows. Each mounted specimen was oriented superior-side uppermost, its outer scleral surface toward the incident x-ray beam and with its natural curvature retained. WAXS patterns, each resulting from an x-ray exposure of between 3 and 5 seconds, were collected at 0.5-mm (horizontal) × 0.5-mm (vertical) intervals covering all but one specimen. The exception was non-glaucoma specimen n4r, for which an 11.5-mm × 11.5-mm raster scan was performed due to time limitations. WAXS patterns were recorded electronically on a charge-coupled device (CCD) detector (ADSC, Poway, CA) placed 550 mm behind the specimen position. Precise translation of the specimen between exposures was achieved using a motorized x-y stage interfaced with the x-ray camera shutter. The focused x-ray beam had a wavelength of 0.09795 nm and horizontal/vertical dimensions of 0.2 mm. After WAXS experiments, each scleral specimen was immediately returned to 4% paraformaldehyde and stored at 4°C for subsequent multiphoton imaging.

The WAXS pattern from sclera is dominated by a well-resolved equatorial (i.e., perpendicular to the fiber axis) reflection from the regular 1.6-nm spacing of the constituent collagen molecules aligned near axially within the scleral fibers (Fig. 1A). Analysis of the angular spread of intensity around this reflection provides a quantitative measure of the relative number of fibers oriented at a given angle within the scleral plane, as an average value within the tissue volume traversed by the x-ray beam.[22] Thus, the method can describe bulk collagen anisotropy in terms of the excess fibers aligned in a given direction over and above the general population that are dispersed equally in all orientations.

The quantification of corneal and scleral collagen fiber orientation from WAXS patterns is described in detail elsewhere.[22] In brief, a two-dimensional background function was firstly fitted and subtracted from each WAXS pattern to remove scatter from the specimen chamber and all other tissue components other than fibrous collagen. For every WAXS pattern, 256 equally spaced radial profiles from pattern center to beyond the collagen signal were generated and a unique power-law background function independently fitted to and subtracted from each (Fig. 1B), using a purpose-written macro routine in a spreadsheet program (Excel; Microsoft Corp., Reading, UK). The isolated collagen scatter peak for each of the 256 angular directions was then normalized against fluctuations in x-ray beam current and exposure time, radially integrated, and the resulting values extracted to angular bins, using a combination of image analysis (Optimas 6.5; Media Cybernetics Inc., Marlow, UK) and spreadsheet software (Microsoft Corp.) software. The resulting angular intensity profile (Fig. 1C) was divided into isotropic and anisotropic scatter components and the latter plotted in polar vector coordinates, introducing a 90° angular shift to account for equatorial scatter. Every sampled point in the sclera could thereby be represented by a polar vector plot (Fig. 1D), in which the length of a vector in any direction gave the relative number of fibers preferentially aligned in that direction, at that point in the tissue. Individual plots were then assimilated into montages showing the preferential fiber orientation across each specimen.

While the vector lengths within a given polar plot give an accurate measure of the relative fiber number for each angle at that point in the tissue, it should be noted that the relative overall size of individual plots between measurement points scales not only with the degree of preferential fiber alignment, but also with scleral thickness.[22] The scaling of the polar plots should therefore be only used as a qualitative guide to the level of collagen alignment. An accurate measure of the degree of fiber anisotropy in the tissue may be gained by computing the ratio of the preferentially aligned and total x-ray scatter to remove the thickness dependency.[22] This was done for every sampled point in the sclera by dividing the integral of the aligned scatter distribution (clear region in Fig. 1B) by the corresponding integral of the total scatter (clear plus shaded regions in Fig. 1B), yielding a single value representing the proportion of fibers preferentially aligned at that point in the tissue. These values were then assimilated into spreadsheet (Microsoft Corp.) contour maps to show the variation in degree of fiber anisotropy across each specimen.

Table 1. Details of the Caucasian Human Sclerae Used in the Study

Sclera	Left/Right	Age	Sex	Non-glaucoma (N)/ Glaucoma (G)	Nerve Grade	Diabetes	Dimensions (SI, NT, AL)
n1l*	L	77	F	N	0	No	24.4, 24.2, 23.9
n1r*	R	77	F	N	0	No	24.4, 24.6, 23.9
n2l	L	74	F	N	0	Type II	24.8, 25.1, 25.3
n3r	R	77	M	N	0	No	24.2, 24.7, 24.8
n4r	R	71	F	N	0	No	23.1, 22.1, 23.5
n5r	R	91	F	N	0	No	22.4, 23.0, 22.7
n6r	R	67	F	N	0	Type I	22.6, 23.0, 23.1
g1l*	L	81	F	G	3	No	24.1, 23.7, 23.4
g1r*	R	81	F	G	3	No	23.4, 23.9, 24.4
g2l	L	82	M	G	3	Type II	25.1, 25.9, 25.2
g3r	R	63	M	G	2	Type II	†
g4r	R	63	M	G	2	No	24.2, 24.5, 24.3

Dimensions refer to superior-inferior and nasal-temporal globe diameters and axial length in mm.
* Left/right pair from the same donor.
† Data not recorded.

Scleral fiber anisotropy was statistically compared between the non-glaucoma and glaucoma groups. For each specimen, the 64 sampling points within a 1.5-mm wide annulus adjacent to the scleral canal were considered as representing the peripapillary sclera (Fig. 2A). Over 98% of the polar vectors plots within this region indicated preferential fiber alignment circumferential to the scleral canal (Fig. 2B). All sampling points lying outside this region were considered midposterior sclera. The peripapillary and midposterior regions were then each subdivided into their four principal quadrants (Fig. 2C) and the mean and variance of each subregion was evaluated per specimen. Midposterior regional averages were not calculated for specimen n4r, due to this being a partial WAXS scan. Pooled anisotropy values within

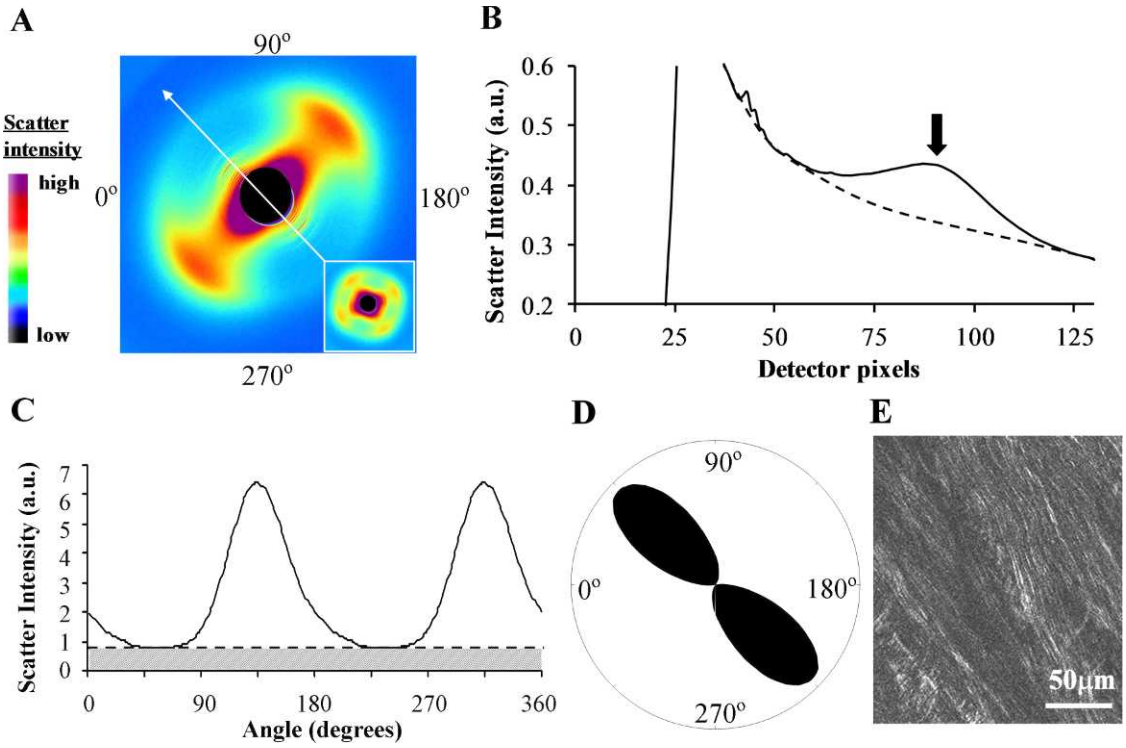

Figure 1. WAXS data analysis. (**A**) WAXS pattern from the peripapillary region of human sclera. The two-lobed appearance of the collagen intermolecular x-ray reflection is indicative of uniaxial fiber alignment in the direction of the *arrow*. *Inset:* Example of a four-lobed WAXS pattern from the midposterior sclera, indicative of biaxial fiber alignment. (**B**) Power-law background function (*broken line*) fitted to a radial profile (*solid line*) through pattern shown in (A). For each pattern, 256 individual such background functions were fitted and subtracted along 256 equally spaced radial directions, enabling the collagen signal to be isolated and extracted in two dimensions. *Arrow:* Collagen signal peak. (**C**) Angular x-ray scatter intensity profile of pattern shown in (A). The scatter may be separated into that arising from isotropically arranged collagen fibers (*shaded region*) and that arising from preferentially oriented fibers (*clear region*). (**D**) Aligned collagen scatter displayed as a polar vector plot, whose shape reveals the collagen anisotropy. The length of any line drawn from the center of the plot to its edge in a given direction is proportional to the relative number of fibers preferentially aligned in that direction. (**E**) Multiphoton microscopy image from mid-stromal depth, taken from the same specimen and region as the WAXS data. Second harmonic generation signals reveal highly aligned collagen fibril bundles, in agreement with the fiber orientation measurement by WAXS.

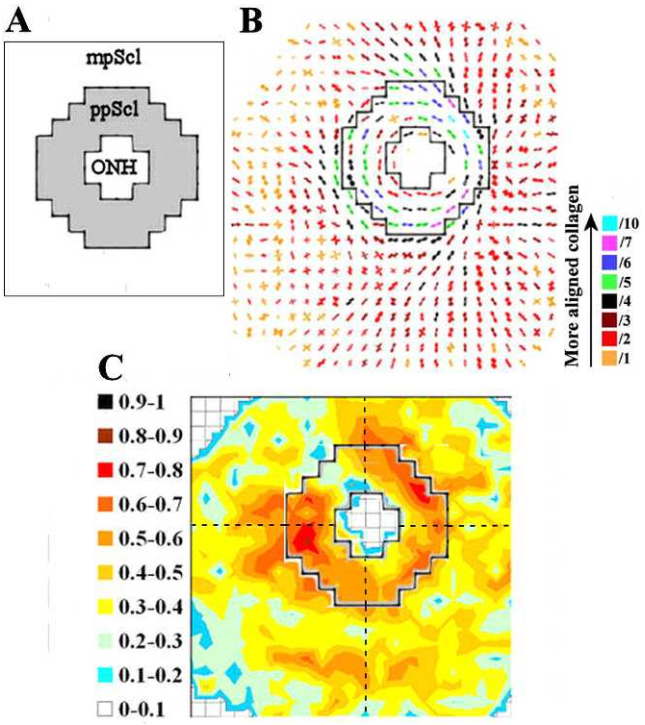

Figure 2. Regional division of sclera for statistical comparison of anisotropy. (**A**) A fixed-size region (*shaded*), encompassing 64 measurement points, representing the peripapillary sclera (ppScl) was identified for each specimen. All data points outside this region were considered midposterior sclera (mpScl). (**B**) ppScl region overlaid on fiber polar vector map for specimen n4r. The ppScl region was identified based on the x-ray scatter dropout in the nerve head and the presence of strong circumferential fiber alignment indicated by the polar vectors. The scaling of the vectors is related to the degree of anisotropy. To allow montage display, the larger plots (indicative of higher fiber anisotropy) have been scaled down by the factors indicated in the color key. (**C**) ppScl region (*solid line*) overlaid on the contour map of calculated fiber anisotropy. The mpScl and ppScl regions were subdivided into their four principal quadrants (*broken lines*); and the mean anisotropy values within each region were statistically compared between non-glaucoma and glaucoma groups.

each of the eight scleral regions were then compared for significant differences between non-glaucoma and glaucoma groups using Welch-corrected two-tailed *t*-test. To account for lower variability between eyes from the same donor, corresponding values within fellow eyes of the non-glaucoma (n1l and n1r) and glaucoma (g1l and g1r) pair were firstly averaged for subsequent statistical analysis.

Multiphoton Microscopy

Although WAXS provides highly quantitative measurements of bulk fiber anisotropy, it cannot tell us how individual fiber bundles are arranged within a given scleral layer, nor how the orientation of fibers changes as a function of tissue depth. Multiphoton microscopy has been widely used to provide qualitative information of this kind from the sclera, including the peripapillary region.[19,21] In order to determine the depth-dependency of fiber orientation in the peripapillary sclera of non-glaucoma and glaucoma eyes, multiphoton imaging was performed on two of the same non-glaucoma (n4r and n6r) and glaucoma (g1l and g3r) specimens previously examined by WAXS. Pilot experiments comparing tissue with and without x-ray exposure verified that WAXS did not result in any disruption or artefact in the resulting multiphoton collagen signal. Full-thickness circular specimens, centered on the optic nerve head, were excised from the fixed posterior-scleral specimens using a 6-mm biopsy punch. The resulting tissue pieces were then separated into six 150-μm thick serial sections using a sledge microtome (HM440E; Microm, Walldorf, Germany) before being slide-mounted in 1:1 PBS/glycerol for maintenance of tissue hydration and refractive index matching. A recent study showed that glycerol treatment does not significantly affect collagen fiber architecture.[21]

Nonlinear laser-scanning multiphoton microscopy was performed using a commercial device (Zeiss LSM 510 META NLO; Carl Zeiss Ltd, Welwyn Garden City, UK). An Ultrafast titanium-sapphire laser (Cameleon; Coherent, Inc., Ely, UK) operating at 800 nm and <140 fs/90 MHz pulses was used to produce second harmonic generation signals from fibrous collagen detected at 400 ± 10 nm in the forward direction (nondescanned detector).[25] A mid-depth image plane was obtained within each section using a 20× 0.8 N.A. objective lens (Plan-Apochromat; Carl Zeiss Ltd), providing a 400-μm × 400-μm field-of-view. A 15 × 15 field-of-view tiling, covering the whole of each section, was then obtained using x-y motor stages (~1.5 hours per section). The resulting datasets were reconstructed using image analyzer software (Zeiss LSM Image Examiner 5.0; Carl Zeiss Microscopy, GmBH, Germany).

Semiquantitative depth profiles of fiber anisotropy in the peripapillary sclera were obtained from the multiphoton images at four separate locations in the peripapillary sclera, one per tissue quadrant. The fast Fourier transform (FFT) processing algorithm (ImageJ; W. Rasband, NIH, Bethesda, MD) was used to generate a theoretical diffraction pattern from each image (Figs. 3A, 3B). The baseline intensity for each FFT pattern was removed, the central 100-pixel radial zone integrated, and the azimuthal intensity distribution extracted to 256 equally spaced bins (Figs. 3B, 3C), using diffraction analysis software (Fit2D; A. P. Hammersley, ESRF, Grenoble, France). Fiber anisotropy plots were then produced for each image by phase-shifting the aligned fiber component of the azimuthal intensity profile (clear region in Fig. 3C) by 90° and displaying the resulting graphs in polar coordinates (Fig. 3D), analogous to the polar vector representation used for the WAXS data. An accompanying anisotropy value was calculated for each plot by computing the ratio of the integrals of the aligned and aligned-plus-isotropic components of the azimuthal intensity distribution (Fig. 3C), following the convention used in the WAXS analysis. Each anisotropy value was then normalized against the maximal value in the sequence to give a measure of the relative degree of circumferential alignment with respect to tissue depth.

Results

X-ray Scattering

Figure 4 shows polar vector maps of preferential collagen fiber orientation in left and right posterior sclerae of a non-glaucoma donor (n1). Supplementary Figure S1 shows equivalent data from the left eye of a second non-glaucoma donor (n2; see Supplementary Material and Supplementary Fig. S1, http://www.iovs.org/lookup/suppl/doi:10.1167/iovs.12-9705/-/DCSupplemental). The maps indicate that fiber orientation in the midposterior sclera was anisotropic and inhomogeneous. Although fiber arrangement was evidently complex, the predominantly 2-fold and 4-fold symmetry of the individual plots indicates that, at any given position, fiber anisotropy could be represented in terms of either one (from here onward referred to as 'uniaxial') or two ('biaxial') preferential fiber directions with associated dispersions. The peripapillary sclera was characterized by a circumferential alignment of fibers parallel to the scleral canal. In addition, notable meridional fiber bands radiated tangentially from the superior and inferior regions of the peripapillary collagen ring in superior-nasal and inferior-nasal directions respectively, rendering a degree of mirror symmetry between left and right eyes (Figs. 4C, 4D [*arrows*]). Although there was some variation in the bulk

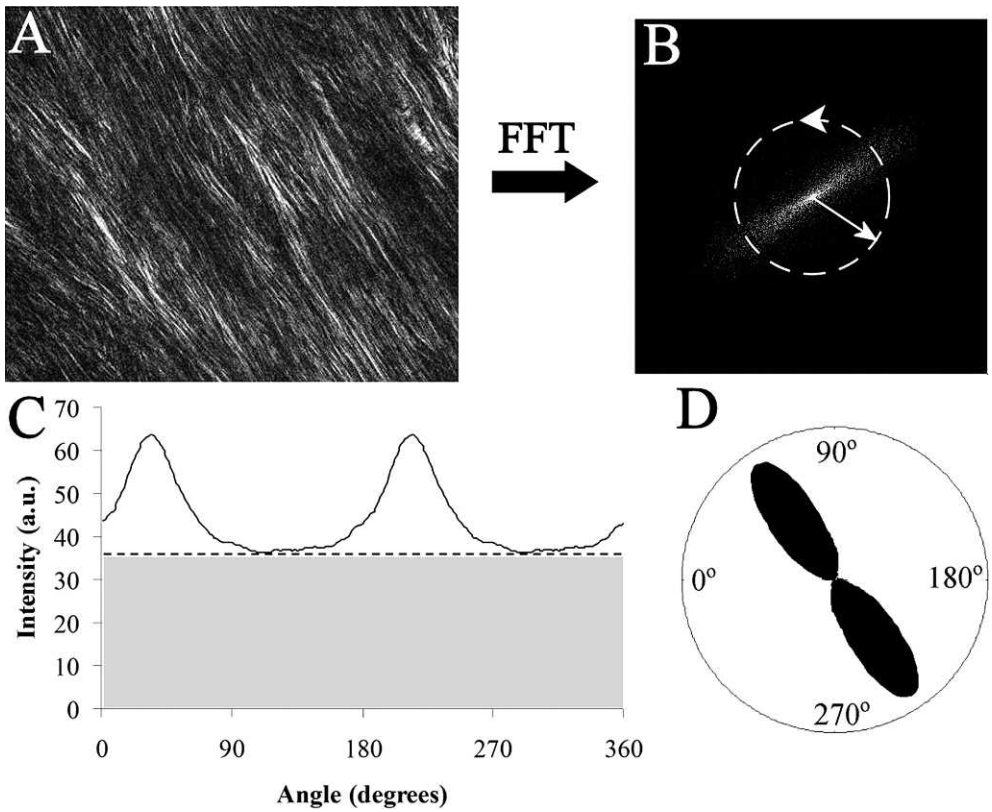

Figure 3. Quantification of fiber anisotropy from collagen SHG signal. (**A**) Multiphoton microscopy image of collagen fibril bundles in the outer stroma of the peripapillary sclera. (**B**) FFT (theoretical diffraction pattern) from image in (**A**). The degree of eccentricity in the pattern relates to degree of fiber alignment. (**C**) Angular intensity profile of FFT shown in (**B**). The distribution may be separated into that arising from isotropically arranged collagen fibers (*shaded region*) and that arising from preferentially oriented fibers (*clear region*). (**D**) Aligned collagen signal displayed as a polar vector plot, whose shape reveals the collagen anisotropy. The length of any line drawn from the center of the plot to its edge in a given direction is related to the relative number of fibers preferentially aligned in that direction.

direction of fibers in the midposterior sclera between individual specimens, these dominant structural features were highly reproducible, and were also found in all four of the remaining non-glaucoma sclerae examined (data not shown). Equivalent polar vector maps from a pair of sclerae from a glaucoma donor (g1), and a left sclera from a second glaucoma donor (g2), are shown in Figures 5 and S2 respectively (see Supplementary Material and Supplementary Fig. S2, http://www.iovs.org/lookup/suppl/doi:10.1167/iovs.12-9705/-/DCSupplemental). The structural features identified in the non-glaucoma specimens were also evident in all five of the glaucoma eyes examined (of which three are shown here). Similar to non-glaucoma specimens, some individual variation in bulk fiber direction was evident in the midposterior sclera. However, no notable overall differences were found between non-glaucoma and glaucoma specimens in terms of bulk fiber direction.

The color-coding of the individual polar vector plots in Figures 4, 5, S1, and S2 suggested that the degree of fiber anisotropy varied with position across each specimen (see Supplementary Material and Supplementary Figs. S1, S2, http://www.iovs.org/lookup/suppl/doi:10.1167/iovs.12-9705/-/DCSupplemental). In general, the peripapillary fiber ring appeared considerably more highly aligned than the midposterior collagen. In order to further quantify this, we computed the anisotropic ratio of aligned to total collagen scatter (Fig. 1C). These values are displayed as contour maps in Figure 6. For both non-glaucoma and glaucoma specimens, the degree of anisotropy was confirmed to be, on average, 37% higher in the peripapillary region compared with the midposterior. Moreover, the degree of anisotropy in the peripapillary ring varied markedly (between 2-fold and 4-fold) with circumferential position around the scleral canal. The distribution pattern of scleral fiber anisotropy varied between specimens within both groups, and this variation was particularly evident in the peripapillary region (Fig. 6). However, minimum peripapillary anisotropy was observed in the superior-nasal quadrant in 6/7 of non-glaucoma and 4/5 of glaucoma sclerae (Fig. 6). Regional and average fiber anisotropy did not differ significantly between non-glaucoma and glaucoma groups in the midposterior sclera (Table 2). In contrast, fiber anisotropy was significantly reduced in the superior-temporal ($P < 0.01$) and inferior-nasal ($P < 0.05$) quadrants of the peripapillary tissue in glaucoma eyes compared with non-glaucoma eyes (Table 2). Regional measures of fiber anisotropy were not statistically different between the four diabetic eyes and the eight nondiabetic eyes studied ($P > 0.05$).

Multiphoton Microscopy

Second harmonic generation signals from fibrous collagen were clearly visible in the peripapillary scleral sections examined using multiphoton imaging (Figs. 7A–F, S). In the inner (i.e., proximal to the choroid) one-third of the peripapillary sclera from non-glaucoma specimen n4r, highly interwoven fibril bundles were observed crossing at random angles (Figs. 7A, 7B). Thereafter, when traversing the tissue thickness in an outward direction, collagen bundles appeared progressively less-interwoven and more highly aligned circum-

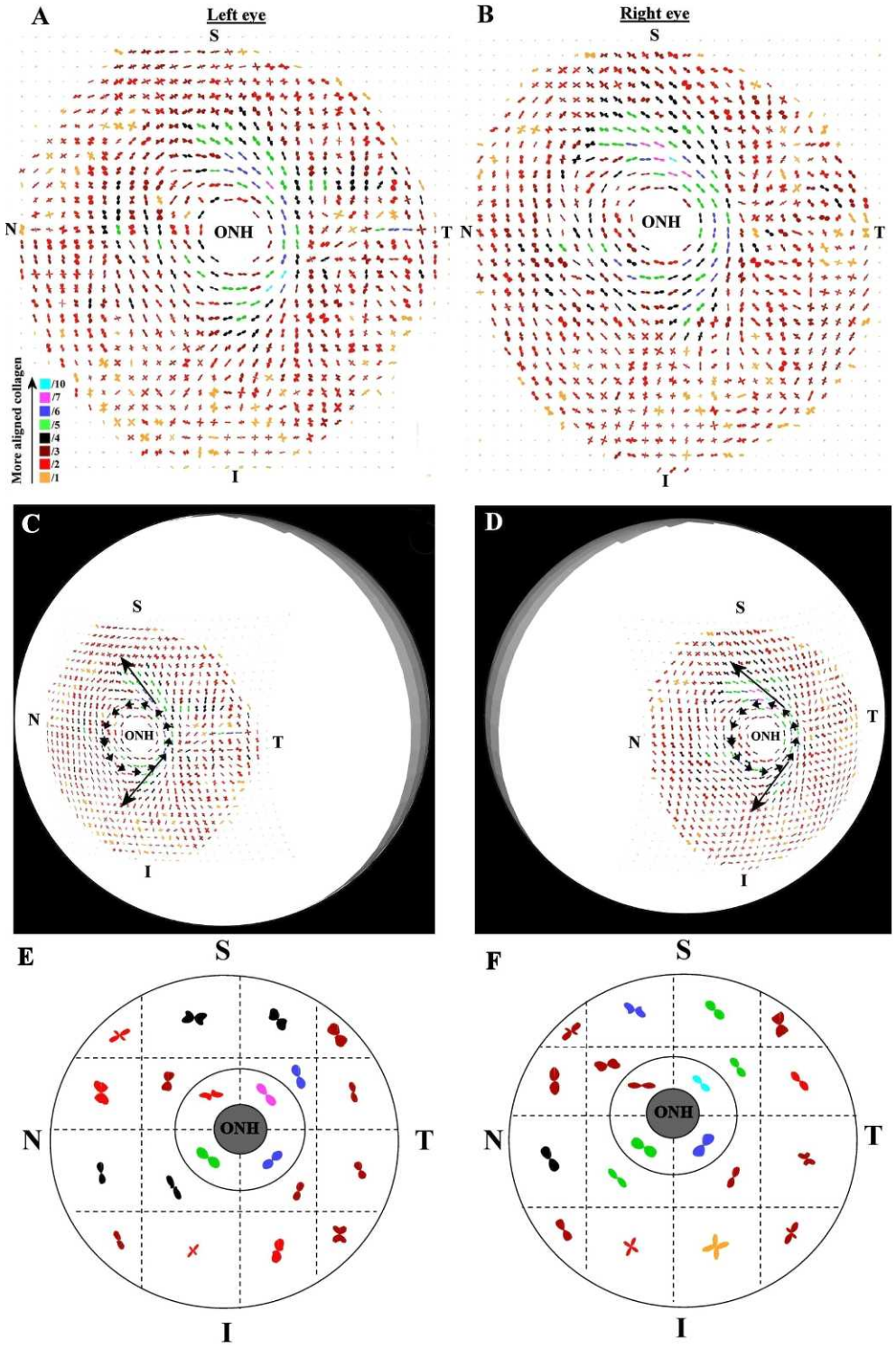

Figure 4. Preferential fiber orientation across non-glaucoma scleral pair. (**A**, **B**) Polar vector maps of preferential collagen fiber orientation across 15-mm diameter posterior scleral specimens (n1l and n1r) from a pair of non-glaucoma human eyes, sampled at 0.5-mm intervals, and viewed from the posterior side. The scaling of the vectors is related to the degree of anisotropy. To allow montage display, the larger plots (indicative of higher fiber anisotropy) have been scaled down by the factors indicated in the color key. Superior (*S*), inferior (*I*), nasal (*N*), and temporal (*T*) specimen positions are marked. The left eye has been mirror-flipped horizontally to enable direct comparison with the right eye. (**C**, **D**) Polar vector plots mapped onto 3-D posterior eye models. Dominant features of the fiber structure are indicated by *arrows:* note circumferential fibers ringing the optic nerve head (ONH) and the oblique splaying of meridional fibers from the ring toward the S-N and I-N directions. **(E**, **F)** Regional maps showing average polar plots within the four principal quadrants of the peripapillary sclera and 16 regions of the midposterior tissue.

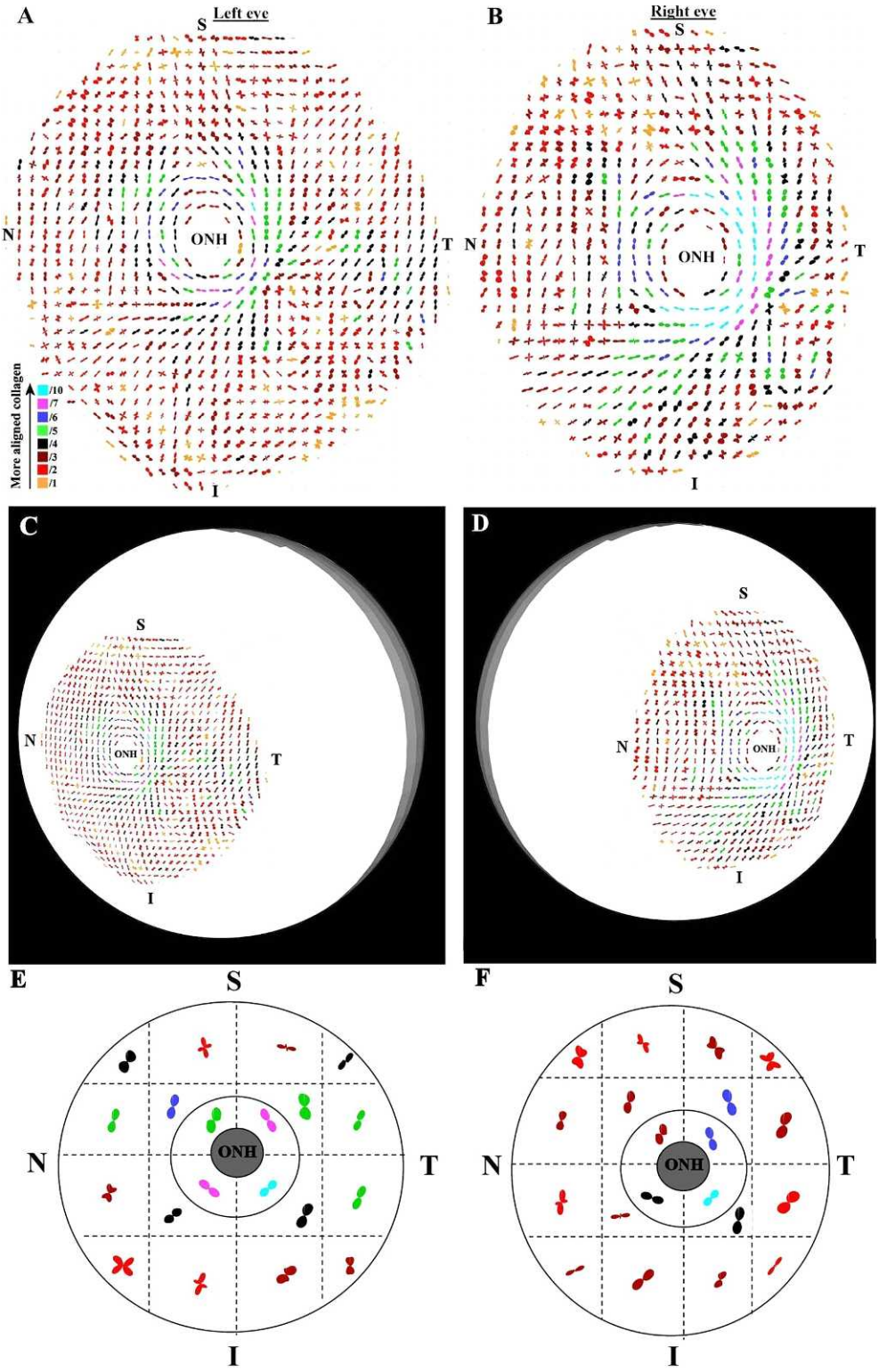

Figure 5. Preferential fiber orientation across glaucoma scleral pair. (**A**, **B**) Polar vector maps of preferential collagen fiber orientation across 15-mm diameter posterior-scleral specimens (g1l and g1r) from a pair of glaucoma human eyes, sampled at 0.5-mm intervals, and viewed from the posterior side. The left eye has been mirror-flipped horizontally to enable direct comparison with the right eye. **(C**, **D)** Polar vector plots mapped onto 3-D posterior eye models. Note the overall arrangement of fibers is similar to non-glaucoma eyes. (**E**, **F**) Regional maps showing average polar plots within the four principal quadrants of the peripapillary sclera and 16 regions of the midposterior tissue.

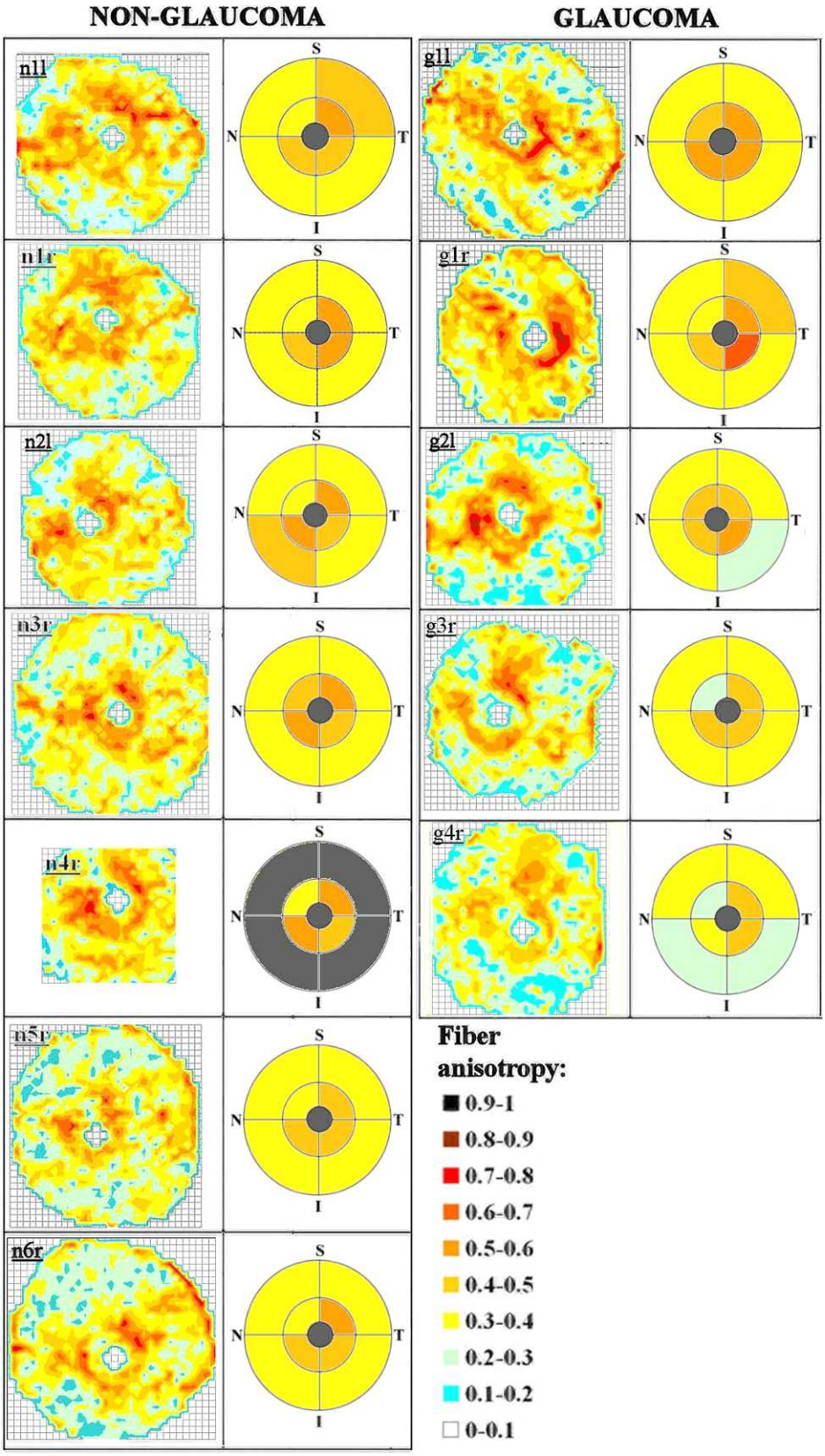

Figure 6. Fiber anisotropy across posterior sclera. *Left panel:* Contour maps of fiber anisotropy for non-glaucoma human posterior sclerae, viewed from the posterior side. The left eyes have been mirror-flipped horizontally to enable direct comparison with the right eyes. Color key shows degree of anisotropy expressed as proportion of aligned to total collagen fiber x-ray scatter. Grid element: 0.5 mm. Mean regional anisotropy within the principal quadrants of the peripapillary and midposterior regions are shown alongside each map. The S, I, N, and T poles are indicated. *Right panel:* Equivalent data for glaucoma specimens. Note the large variation in peripapillary anisotropy with position around the scleral canal for both groups. Midposterior regional averages are not shown for specimen n4r due to this being a partial WAXS scan.

ferential to the scleral canal (Figs. 7C–E) before becoming less aligned again in the most superficial one-sixth of the sclera (Fig. 7F). FFT analysis of multiphoton images confirmed fiber anisotropy was higher in the mid-to-outer stroma compared to the inner sclera (Figs. 7G–L, M–R), with peak anisotropy always occurring in the depth range: 200 to 500 μm (Fig. 7T). A similar trend was observed in the peripapillary sclera of glaucoma specimen g3r (Fig. 8). These features were confirmed in a further specimen from each group, n6r and g1l (see Supplementary Material and Supplementary Fig. S3, http://www.iovs.org/lookup/suppl/doi:10.1167/iovs.12-9705/-/DCSupplemental). Mean and standard deviations for the depth at which peak fiber anisotropy was observed, per eye, were: n4r (388 μm ± 144); n6r (350 μm ± 123); g3r (275 μm ± 87); g1l (300 μm ± 87). Further experimental work, using a larger multiphoton specimen size, is required to determine whether the depth dependency of the fiber orientation varies significantly between non-glaucoma and glaucoma eyes.

Discussion

The WAXS results presented here indicate that the human posterior sclera is highly anisotropic, and that both the direction and degree of anisotropy vary markedly across the tissue. This fits well with mechanical[26,27] and histological findings[16] in human eyes. Our reporting of biaxial preferential fiber alignment in regions of the midposterior sclera (Figs. 4, 5, S1, and S2; see Supplementary Material and Supplementary Figs. S1, S2, http://www.iovs.org/lookup/suppl/doi:10.1167/iovs.12-9705/-/DCSupplemental) is likely due to bands of collagen at various depths in the tissue crossing at large angles, as implied by Kokott's early work.[16] With this in mind, it should be remembered that our WAXS method yields thickness-averaged data and cannot reveal depth-dependent information. Moreover, multiple collagen bands crossing at more acute angles may be assimilated by WAXS into a common distribution about a single dominant preferred direction. In these respects, WAXS presents a highly quantitative yet simplified view of the full tissue architecture.

Our observation of a highly reinforced circumferential ring of collagen fibers in the peripapillary sclera (Figs. 4, 5, S1, and S2; see Supplementary Material and Supplementary Figs. S1, S2, http://www.iovs.org/lookup/suppl/doi:10.1167/iovs.12-9705/-/DCSupplemental) is consistent with previous qualitative imaging of human tissue.[16,20,28] Such an arrangement is also predicted by measurements of IOP-driven scleral deformation in monkeys[29] and humans.[12] It is possible that this ring forms some protective function for the optic nerve axons, since numerical modeling has shown that a circular arrangement of fibers around the scleral canal is biomechanically optimal in order to minimize lamina expansion as IOP is altered.[30] The oblique meridional fibers associated with the superior and inferior peripapillary sclera (Figs. 4, 5, S1, and S2; see Supplementary Material and Supplementary Figs. S1, S2, http://www.iovs.org/lookup/suppl/doi:10.1167/iovs.12-9705/-/DCSupplemental) are also consistent with early histological observations,[16] and may conceivably have some additional stabilizing role in relation to the optic nerve head.

A further interesting result of the current study was that the degree of fiber anisotropy within the peripapillary ring varied markedly (up to 4-fold) with circumferential position around the scleral canal (Fig. 6), and that weakest circumferential alignment was consistently observed in the superior-nasal quadrant (Fig. 6 and Table 2). Moreover, the multiphoton imaging we carried out revealed that this structure does not extend through the full thickness of the tissue, but instead is formed mainly by fibers lying in the mid-to-outer stroma and encompassing only approximately 50% of the total scleral thickness (Figs. 7, 8). We suggest that there would be some value in considering these features in future numerical simulations aimed at predicting IOP-derived lamina strain.

Table 2. Comparison of Collagen Fiber Anisotropy by Scleral Region between Non-glaucoma and Glaucoma Groups, as Measured Using WAXS.

	Non-glaucoma		Glaucoma	
Region	**Mean**	**Var.**	**Mean**	**Var.**
MP-SN	0.32	(0.02)	0.35	(0.02)
MP-ST	0.36	(0.02)	0.35	(0.02)
MP-IN	0.34	(0.01)	0.32	(0.02)
MP-IT	0.33	(0.02)	0.31	(0.05)
MP-all	0.34	(0.02)	0.33	(0.02)
PP-SN	0.39	(0.03)	0.37	(0.02)
PP-ST	0.55	(0.01)†	0.47	(0.03)†
PP-IN	0.49	(0.01)*	0.45	(0.01)*
PP-IT	0.46	(0.01)	0.50	(0.02)
PP-all	0.47	(0.02)	0.45	(0.02)

MP, midposterior sclera; PP, peripapillary sclera; SN, superior-nasal quadrant; ST, superior-temporal quadrant; IN, inferior-nasal quadrant; IT, inferior-temporal quadrant.

* $P < 0.05$.

† $P < 0.01$.

There is evidence that connective tissue remodeling in glaucoma extends beyond the lamina into the peripapillary sclera.[11,13–15] Notably, studies of glaucomatous human eyes using electron microscopy have indicated a decrease in peripapillary collagen fibril density[15] and an uncoupling of the elastin and collagen matrix components.[14] Whether this apparent remodeling extends to the level of collagen fiber alignment has not been addressed experimentally. The current study indicated that the general pattern of bulk fiber directions in posterior human sclera was similar between non-glaucoma donors and those with a history of glaucoma and confirmed axon loss (Figs. 4, 5, S1, and S2; see Supplementary Material and Supplementary Figs. S1, S2, http://www.iovs.org/lookup/suppl/doi:10.1167/iovs.12-9705/-/DCSupplemental). In the context of our observation, it is interesting to note that a recent modeling study using monkey sclera has also suggested no change in bulk fiber direction between non-glaucoma and glaucoma eyes.[31] However, the present study did indicate significant regional differences in mean fiber anisotropy within the peripapillary sclera between non-glaucoma and glaucoma eyes; while, in contrast, no such differences were found in the midposterior tissue (Table 2). It is possible that these differences represent some adaptive change in response to glaucoma, or else might be baseline structural properties that associate with predisposition to glaucomatous axon damage. The course of scleral fibers within a given eye cannot be compared before and after glaucoma onset in a human postmortem study such as ours, and therefore the current results can neither confirm nor distinguish between these two possible interpretations. Further studies characterizing the time-course of fiber anisotropy during disease development in experimental glaucoma are encouraged.

The regional differences in peripapillary fiber anisotropy between normal and damaged glaucoma eyes identified herein may be relevant biomechanically. Of interest, a recent study reported differing meridional strain behavior in the peripapillary region of age-matched control and damaged glaucoma human sclerae subjected to inflation tests, while midposterior stress-strain behavior was similar between the groups.[12] With this in mind, it is relevant to note that the mechanical stiffness

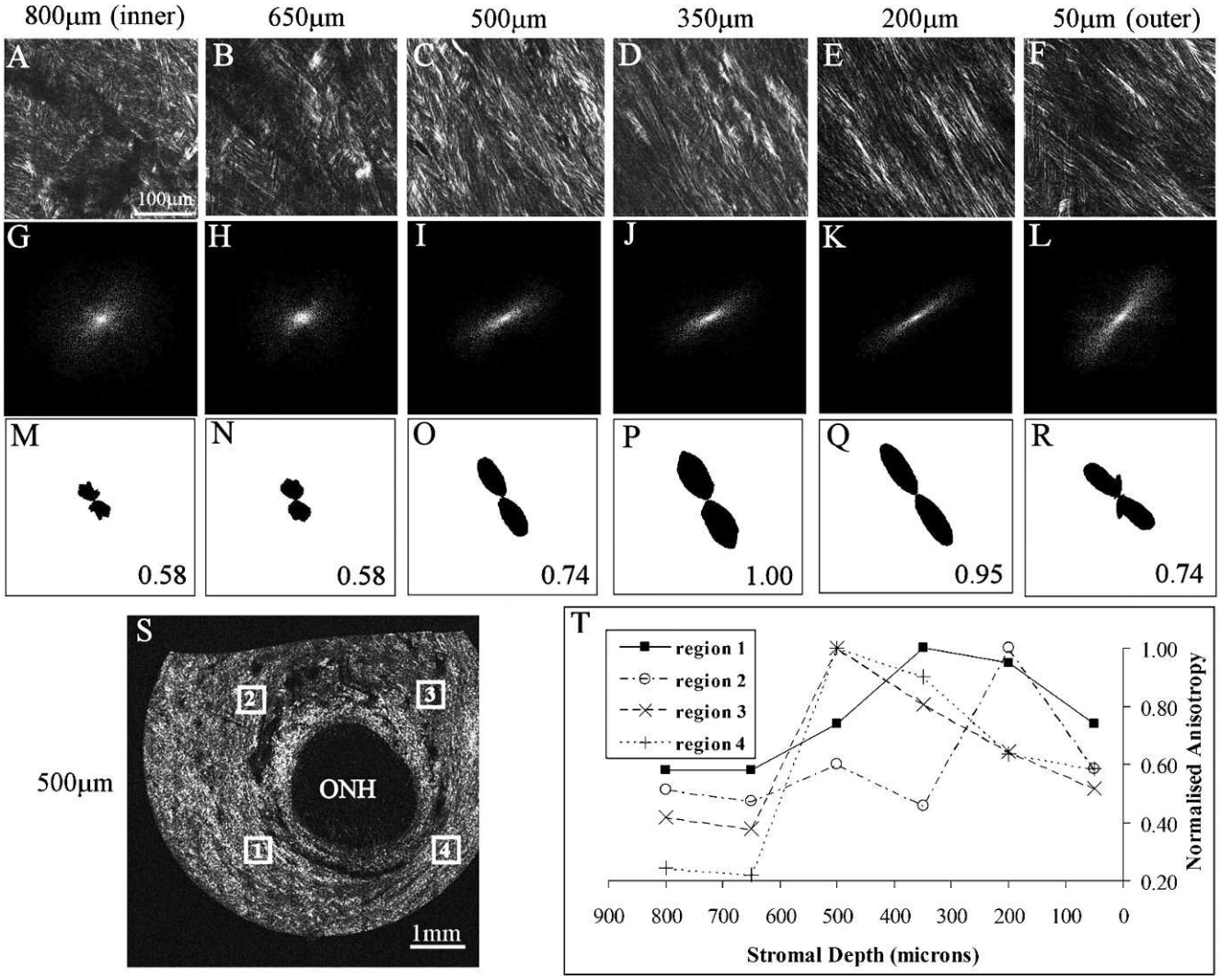

Figure 7. Second harmonic generation multiphoton imaging of non-glaucoma peripapillary sclera. (**A–F**) Multiphoton images from peripapillary sclera of non-glaucoma human eye n4r; second harmonic generation signals reveal collagen fibril bundle arrangement. The left-to-right image sequence shows a depth profile at a single location (*region 1 in panel S*), traversing the scleral thickness in an inner (choroid side) to outer direction at the depths indicated. Note that mid-/outer stromal collagen fibril bundles are less interwoven and more highly aligned in (**C–E**) before becoming less aligned in the outermost layer in (**F**). (**G–L**) FFT (theoretical diffraction patterns) calculated from the images (**A–F**). The eccentricity of the patterns is related to the degree of fiber anisotropy. (**M–R**) Polar vector plots of preferential fiber orientation, calculated from FFTs. The same scaling was used for all plots. Relative anisotropy (normalized to the maximum value in the sequence) is shown alongside each plot. (**S**) Reconstruction of 15×15 multiphoton image tiling of whole peripapillary sclera at a depth of 500 μm, showing fibrillar collagen circumferential to the ONH. The *white rectangles* denote the four locations at which the depth-profiles were recorded. (**T**) Graph showing normalized fiber anisotropy as a function of tissue depth at the four locations shown in *panel S*.

of the sclera, or its resistance to deformation, is influenced by both geometric and material parameters.[5,6,31] Further research is required to determine exactly how the interplay between scleral size, shape, thickness, and fiber arrangement within a given eye governs its individual response to IOP change, particularly given the inter-specimen variations in fiber anisotropy indicated by the current WAXS data.

As mentioned above, it is important to note that the WAXS method we have used here is inherently limited in its inability to determine the depth dependency of the preferred orientation of scleral collagen. Quantitative depth-profiling of sclera is potentially achievable by combining WAXS with serial tissue sectioning, as demonstrated by corneal studies.[32,33] In addition, our study was subject to a number of further experimental limitations. Firstly, there was the effect of the scleral curvature. With increasing distance from the nerve head, the effective tissue thickness presented to the x-ray beam is increasingly elevated by the curvature, with a proportional increase in total (i.e., isotropic and aligned) x-ray scatter, affecting the relative size of the polar vector plots in Figures 4, 5, S1, and S2 (see Supplementary Material and Supplementary Figs. S1, S2, http://www.iovs.org/lookup/suppl/doi:10.1167/iovs.12-9705/-/DCSupplemental). The estimated increase in scatter due to scleral curvature was calculated to be $<2\%$ in the peripapillary region, increasing to $\sim 17\%$ at the specimen periphery (based on a posterior-scleral radius of curvature of 12 mm). However, it is important to note that curvature would not have affected the relative fiber number as a function of angle within a given polar vector plot (indicated by the shape of the individual plots). Neither would it have affected the fiber

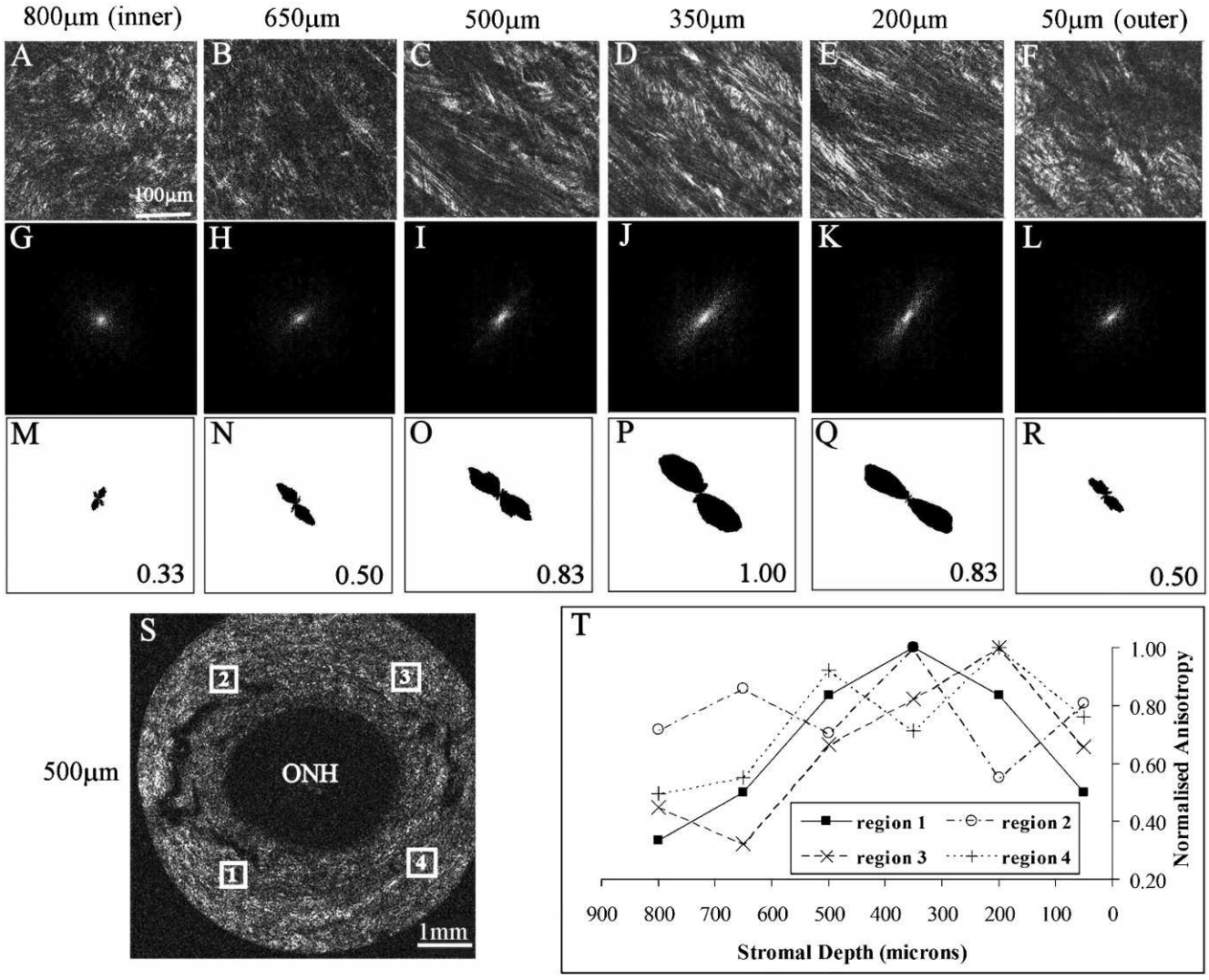

Figure 8. Second harmonic generation multiphoton imaging of glaucoma peripapillary sclera. (**A–F**) Multiphoton image depth profile from peripapillary sclera of glaucoma human eye g3r, recorded from region 1 (see *panel S* for location). (**G–L**) FFTs (theoretical diffraction patterns) of images shown (**A–F**). (**M–R**) Polar vector plots and normalized anisotropy values calculated from FFTs. The same scaling was used for all plots. (**S**) Reconstruction of whole peripapillary sclera at a depth of 500 μm. The *white rectangles* denote the four locations at which the depth-profiles were recorded. (**T**) Graph showing normalized fiber anisotropy as a function of tissue depth at the four locations shown in (**8S**). Note that the depth-dependency of the fiber anisotropy follows that of the non-glaucoma specimen.

anisotropy measurements (Fig. 6), which are thickness-independent.[22] To characterize fiber orientation across the whole posterior sclera without dissection will require a tilting specimen cell to maintain the incident x-ray beam perpendicular to the tissue surface. This is currently under development.

The second limitation concerns the hierarchical structure of collagen. Since WAXS is a molecular signal,[22] the helicoidal packing of the microfibrillar subunits comprising the fibers will contribute to the angular smearing of the WAXS diffraction peaks shown in Figure 1A, leading to an underestimation in the degree of fiber anisotropy measured by WAXS. In sclera the microfibrillar tilt angle with respect to the fiber axis is relatively small (~5°),[18] and therefore we anticipate our underestimation of anisotropy by WAXS to be accordingly minor. The multiphoton signal derives from fibril bundles, and is therefore not subject to this error. However, the difference in signal origin should be borne in mind when comparing data from the WAXS and multiphoton methods. The size of collagen fibril bundle structures detected by multiphoton imaging is highly variable, predicting a radially diffuse FFT pattern (see Figs. 7, 8), whereas WAXS has the advantage that the collagen molecular diameter is, in contrast, highly uniform, leading to a much sharper, more well-resolved signal (see Fig. 1). Moreover, a proportion of the fibrillar structures in the multiphoton images are obscured to the FFT processing by the interwoven nature of the sclera (Figs. 7, 8), whereas WAXS is not affected. Owing to these limitations, in the current paper quantification of fiber anisotropy from multiphoton data is limited to reporting of relative, normalized values only. Any study that makes a comparison between absolute values of fiber anisotropy as measured using imaging and scattering methods should consider the above-mentioned factors.

Thirdly, it is likely that some, if not all, of the human sclerae used in this study were from donors affected with varying degrees of refractive error. It is unknown whether bulk scleral fiber orientation is affected in myopia. However, there is extensive evidence from both human and animal myopia studies that the posterior-scleral matrix remodels at the level of the collagen fibrils during myopic eye growth.[34,35] While refractive information was not available for the sclerae used in

our study, measurements of ocular dimensions post-mortem did not indicate any significant differential trend between the non-glaucoma and glaucoma groups (Table 1). Nevertheless, it is possible that interspecimen differences in myopic status may have made some contribution to the large differences in anisotropy between eyes indicated herein.

Lastly, there are inherent difficulties in confirming glaucoma status in human eyes obtained post-mortem from eye bank sources. Many previous studies have accepted the statement from the providing agency that the patient had glaucoma, owing to increasing difficulties in obtaining detailed medical records of glaucoma diagnosis and treatment due to federal privacy regulations. In a recent publication,[12] we evaluated optic nerve cross-sections of glaucoma eyes using a previously validated histological method,[24] and were able to assess the severity of axonal damage in 20 out of 24 specimens. The ungradable nerves suffered post-mortem autolysis. We have used the same methodology here to verify glaucoma status in eyes obtained from NDRI. Other investigators are encouraged to perform optic nerve damage assessment by some histological method to validate glaucoma status in the eye bank tissues that they use.

In summary, we have used WAXS and multiphoton imaging to quantitatively map the orientation of collagen in the peripapillary and midposterior human sclera, showing that the bulk fiber arrangement at any given point in the tissue can be simplified into uniaxial or biaxial distributions. As such, the data is highly amenable for inclusion in inverse finite-element simulation. Given the considerable variation in anisotropy between specimens highlighted by the current study, we suggest that experimental fiber orientation data should be assimilated into human eye models, along with associated morphometric and thickness parameters, on an individual-specific basis. This work is currently ongoing in our lab. Quantitative structural information on human sclera of the kind presented here will help to improve our understanding of the tissue's mechanical influence on the optic nerve head, and thereby the sclera's possible role in glaucoma.

Acknowledgments

The authors thank Nick White of Vision Sciences Bioimaging Laboratories, Cardiff University, for advice concerning the nonlinear microscopy.

References

1. Watson PG, Young RD. Scleral structure, organisation and disease. A review. *Exp Eye Res*. 2004;78:609–623.
2. Girard MJ, Downs JC, Bottlang M, Burgoyne CF, Suh JK. Peripapillary and Posterior Scleral Mechanics-Part II: Experimental and Inverse Finite Element Characterization. *J Biomech Eng*. 2009;131:051012.
3. Burgoyne CF, Downs JC. Premise and prediction-how optic nerve head biomechanics underlies the susceptibility and clinical behavior of the aged optic nerve head. *J Glaucoma*. 2008;17:318–328.
4. Downs JC, Roberts MD, Burgoyne CF. Mechanical environment of the optic nerve head in glaucoma. *Optom Vis Sci*. 2008;85:425–435.
5. Eilaghi A, Flanagan JG, Simmons CA, Ethier CR. Effects of scleral stiffness properties on optic nerve head biomechanics. *Ann Biomed Eng*. 2010;38:1586–1592.
6. Norman RE, Flanagan JG, Sigal IA, Rausch SM, Tertinegg I, Ethier CR. Finite element modeling of the human sclera: influence on optic nerve head biomechanics and connections with glaucoma. *Exp Eye Res*. 2011;93:4–12.
7. Sigal IA, Flanagan JG, Tertinegg I, Ethier CR. Modeling individual-specific human optic nerve head biomechanics. Part II: influence of material properties. *Biomech Model Mechanobiol*. 2009;8:99–109.
8. Sigal IA, Ethier CR. Biomechanics of the optic nerve head. *Exp Eye Res*. 2009;88:799–807.
9. Quigley HA, Addicks EM, Green WR, Maumenee AE. Optic nerve damage in human glaucoma. II. The site of injury and susceptibility to damage. *Arch Ophthalmol*. 1981;99:635–649.
10. Sigal IA. Interactions between geometry and mechanical properties on the optic nerve head. *Invest Ophthalmol Vis Sci*. 2009;50:2785–2795.
11. Norman RE, Flanagan JG, Rausch SM, et al. Dimensions of the human sclera: Thickness measurement and regional changes with axial length. *Exp Eye Res*. 2010;90:277–284.
12. Coudrillier B, Tian J, Alexander S, Myers KM, Quigley HA, Nguyen TD. Mechanical response of the human posterior sclera: age and glaucoma related changes measured using inflation testing. *Invest Ophthalmol Vis Sci*. 2012;53:1714–1728.
13. Downs JC, Suh JK, Thomas KA, Bellezza AJ, Hart RT, Burgoyne CF. Viscoelastic material properties of the peripapillary sclera in normal and early-glaucoma monkey eyes. *Invest Ophthalmol Vis Sci*. 2005;46:540–546.
14. Quigley HA, Brown A, Dorman-Pease ME. Alterations in elastin of the optic nerve head in human and experimental glaucoma. *Br J Ophthalmol*. 1991;75:552–557.
15. Quigley HA, Dorman-Pease ME, Brown AE. Quantitative study of collagen and elastin of the optic nerve head and sclera in human and experimental monkey glaucoma. *Curr Eye Res*. 1991;10:877–888.
16. Kokott W. Das spaltlinienbild der sklera (Ein beitrag zum funktionellen bau der sklera). *Klin Monbl Augenheilkd*. 1934;92:177–185.
17. Marshall GE, Konstas AGP, Lee WR. Collagens in ocular tissues. *Br J Ophthalmol*. 1993;77:515–524.
18. Yamamoto S, Hashizume H, Hitomi J, et al. The subfibrillar arrangement of corneal and scleral collagen fibrils as revealed by scanning electron and atomic force microscopy. *Arch Histol Cytol*. 2000;63:127–135.
19. Yan D, McPheeters S, Johnson G, Utzinger U, Vande Geest JP. Microstructural differences in the human posterior sclera as a function of age and ethnicity. *Invest Ophthalmol Vis Sci*. 2011;52:821–829.
20. Winkler M, Jester B, Nien-Shy C, et al. High resolution three-dimensional reconstruction of the collagenous matrix of the human optic nerve head. *Brain Res Bull*. 2010;81:339–348.
21. Girard MJ, Dahlmann-Noor A, Rayapureddi S, et al. Quantitative mapping of scleral fiber orientation in normal rat eyes. *Invest Ophthalmol Vis Sci*. 2011;52:9684–9693.
22. Meek KM, Boote C. The use of x-ray scattering techniques to quantify the orientation and distribution of collagen in the corneal stroma. *Prog Retin Eye Res*. 2009;28:369–392.
23. Boote C, Hayes S, Abahussin M, Meek KM. Mapping collagen organization in the human cornea: left and right eyes are structurally distinct. *Invest Ophthalmol Vis Sci*. 2006;47:901–908.
24. Kendell KR, Quigley HA, Kerrigan LA, Pease ME, Quigley EN. Primary open angle glaucoma is not associated with photoreceptor loss. *Invest Ophthalmol Vis Sci*. 1995;36:200–205.
25. Boote C, Elsheikh A, Kassem W, et al. The influence of lamellar orientation on corneal material behavior: biomechanical and structural changes in an avian corneal disorder. *Invest Ophthalmol Vis Sci*. 2011;52:1243–1251.
26. Bisplinghoff JA, McNally C, Manoogian SJ, Duma SM. Dynamic material properties of the human sclera. *J Biomech*. 2009;42:1493–1497.

27. Elsheikh A, Geraghty B, Alhasso D, Knappett J, Campanelli M, Rama P. Regional variation in the biomechanical properties of the human sclera. *Exp Eye Res*. 2010;90:624–633.
28. Morrison JC, Lhernault NL, Jerdan JA, Quigley HA. Ultrastructural location of extracellular-matrix components in the optic nerve head. *Arch Ophthalmol*. 1989;107:123–129.
29. Girard MJ, Suh JK, Bottlang M, Burgoyne CF, Downs JC. Scleral biomechanics in the aging monkey eye. *Invest Ophthalmol Vis Sci*. 2009;50:5226–5237.
30. Grytz R, Meschke G, Jonas JB. The collagen fibril architecture in the lamina cribrosa and peripapillary sclera predicted by a computational remodeling approach. *Biomech Model Mechanobiol*. 2011;10:371–382.
31. Girard MJ, Suh JK, Bottlang M, Burgoyne CF, Downs JC. Biomechanical changes in the sclera of monkey eyes exposed to chronic IOP elevations. *Invest Ophthalmol Vis Sci*. 2011;52:5656–5659.
32. Abahussin M, Hayes S. Knox Cartwright NE, et al. 3D collagen orientation study of the human cornea using X-ray diffraction and femtosecond laser technology. *Invest Ophthalmol Vis Sci*. 2009;50:5159–5164.
33. Kamma-Lorger CS, Boote C, Hayes S, et al. Collagen and mature elastic fibre organisation as a function of depth in the human cornea and limbus. *J Struct Biol*. 2010;169:424–430.
34. McBrien NA, Jobling AI, Gentle A. Biomechanics of the sclera in myopia: extracellular and cellular factors. *Optom Vis Sci*. 2009;86:E23–E30.
35. Rada JAS, Shelton S, Norton TT. The sclera and myopia. *Exp Eye Res*. 2006;82:185–200.